



## Late Holocene volcanic and anthropogenic mercury deposition in the western Central Andes (Lake Chungará, Chile)

S. Guédron <sup>a,b,\*</sup>, J. Tolu <sup>c,d</sup>, E. Brisset <sup>a,e,f</sup>, P. Sabatier <sup>g</sup>, V. Perrot <sup>a</sup>, S. Bouchet <sup>h,i</sup>, A.L. Develle <sup>g</sup>, R. Bindler <sup>c</sup>, D. Cossa <sup>a</sup>, S.C. Fritz <sup>i</sup>, P.A. Baker <sup>j</sup>

<sup>a</sup> Univ. Grenoble Alpes, Univ. Savoie Mont Blanc, CNRS, IRD, IFSTTAR, ISTerre, 38000 Grenoble, France

<sup>b</sup> Laboratorio de Hidroquímica, Instituto de Investigaciones Químicas, Universidad Mayor de San Andres, Campus Universitario de Cota Cota, casilla 3161, La Paz, Bolivia

<sup>c</sup> Department of Ecology and Environmental Science, Umeå University, Sweden

<sup>d</sup> Eawag, Swiss Federal Institute of Aquatic Science and Technology, CH-8600 Dübendorf, Switzerland and ETH Zürich, Universitätstrasse 16, CH-8092 Zürich, Switzerland

<sup>e</sup> IPHES, Institut Català de Paleoecología Humana i Evolució Social, Tarragona, Spain

<sup>f</sup> Àrea de Prehistòria, Universitat Rovira i Virgili, Tarragona, Spain

<sup>g</sup> Environnement, Dynamique et Territoires de Montagne (EDYTEM), Université Savoie Mont Blanc, CNRS, 73373 Le Bourget du Lac, France

<sup>h</sup> LCABIE – Laboratoire de Chimie Analytique Bio-Inorganique et Environnement, IPREM UMR 5254, CNRS et Université de Pau et des Pays de l'Adour, Hélioparc, F-64053 Pau, France

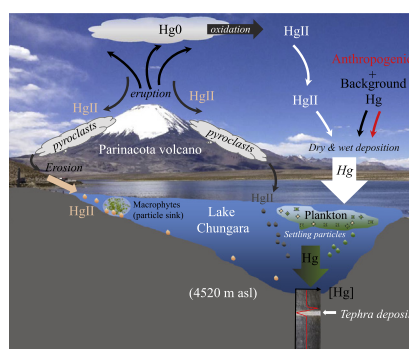
<sup>i</sup> Department of Earth and Atmospheric Sciences, University of Nebraska-Lincoln, Lincoln, NE, USA

<sup>j</sup> Division of Earth and Ocean Sciences, Duke University, Durham, NC, USA

### HIGHLIGHTS

- We studied mercury deposition in Lake Chungará ( $18^{\circ}\text{S}$ ) over the last ~2700 years.
- Parinacota volcano produced 20 tephra layers recorded in lake sediments.
- Lake primary production was the main, not limiting, carrier of Hg to the sediment.
- Volcanoes contributed to ~30% of Hg inputs to the lake over the study period.
- Last 400 years anthropogenic Hg emissions overwhelmed the volcanic activities.

### GRAPHICAL ABSTRACT



### ARTICLE INFO

#### Article history:

Received 16 November 2018

Received in revised form 22 January 2019

Accepted 22 January 2019

Available online 24 January 2019

#### Keywords:

Mercury

Paleolimnology

Holocene

Anthropogenic activities and volcanism

Organic biomarkers

### ABSTRACT

Volcanism is one of the major natural processes emitting mercury (Hg) to the atmosphere, representing a significant component of the global Hg budget. The importance of volcanic eruptions for local-scale Hg deposition was investigated using analyses of Hg, inorganic elemental tracers, and organic biomarkers in a sediment sequence from Lake Chungará (4520 m a.s.l.). Environmental change and Hg deposition in the immediate vicinity of the Parinacota volcano were reconstructed over the last 2700 years, encompassing the pre-anthropogenic and anthropogenic periods. Twenty eruptions delivering large amounts of Hg ( $1$  to  $457 \mu\text{g Hg m}^{-2} \text{yr}^{-1}$  deposited at the timescale of the event) were locally recorded. Peaks of Hg concentration recorded after most of the eruptions were attributed to a decrease in sedimentation rate together with the rapid re-oxidation of gaseous elemental Hg and deposition with fine particles and incorporation into lake primary producers. Over the study period, the contribution of volcanic emissions has been estimated as 32% of the total Hg input to the lake. Sharp depletions in primary production occurred at each eruption, likely resulting from massive volcaniclastic inputs and changes in the lake-water physico-chemistry. Excluding the volcanic deposition periods, Hg accumulation rates rose from natural background values ( $1.9 \pm 0.5 \mu\text{g m}^{-2} \text{yr}^{-1}$ ) by a factor of 2.3 during the pre-colonial mining period

\* Corresponding author at: Univ. Grenoble Alpes, Univ. Savoie Mont Blanc, CNRS, IRD, IFSTTAR, ISTerre, 38000 Grenoble, France.

E-mail address: [stephane.guedron@ird.fr](mailto:stephane.guedron@ird.fr) (S. Guédron).

(1400–900 yr cal. BP), and by a factor of 6 and 7.6, respectively, during the Hispanic colonial epoch (400–150 yr cal. BP) and the industrial era (~140 yr cal. BP to present). Altogether, the dataset indicates that lake primary production has been the main, but not limiting, carrier for Hg to the sediment. Volcanic activity and climate change are only secondary drivers of local Hg deposition relative to the magnitude of regional and global anthropogenic emissions.

© 2019 Elsevier B.V. All rights reserved.

## 1. Introduction

Mercury (Hg) is a global pollutant transported in its gaseous elemental form over long distances in the atmosphere (Pirrone and Mason, 2009). Almost 5 kilotonnes (kt) Hg (Selin, 2009; Mason et al., 2012; Outridge et al., 2018) are contained in the atmosphere, representing the primary source of inorganic Hg for aquatic and terrestrial ecosystems, except for specific areas influenced by specific geological background and/or human activities, such as mining areas (Malm et al., 1995; Guédron et al., 2018a).

Recent global inventories estimated that the pool of atmospheric Hg resulting from natural processes accounts for ~0.8 kt and represents about 18% of the total atmospheric Hg pool (Pacyna et al., 2006; Pirrone et al., 2010; Outridge et al., 2018). Volcanoes are considered to be important natural contributors to the atmospheric Hg pool, at both global and regional scales, through the emission of gaseous elemental Hg [i.e., GEM or  $Hg(0)_g$ ] (Pyle and Mather, 2003; Bagnato et al., 2014; Gustin et al., 2008)]. Submarine volcanism is also a source of Hg, but is not considered significant (Stoffers et al., 1999; Lamborg et al., 2002). Estimates of global volcanic Hg emissions to the atmosphere range over four orders of magnitude, but most realistic values range between 75 and 700  $Mg\ yr^{-1}$  (Varekamp and Buseck, 1986; Ferrara et al., 2000; Nriagu and Becker, 2003; Pyle and Mather, 2003; Gustin et al., 2008; Lohman et al., 2008). Large spatial and temporal variability of volcanism, associated with a paucity of appropriate quantification of Hg (Gustin et al., 2008), make estimates of global volcanic Hg emissions difficult. About 75% of the emitted volcanic  $Hg(0)_g$  may be released during modest-scale sporadic eruptions ( $<10\text{--}10^2\ Mg$  per event), whereas large explosive eruptions ( $>10^3\ Mg$  per event) and continuous degassing may account for 15 and 10%, respectively (Pyle and Mather, 2003; Bagnato et al., 2014). Although part of the emitted  $Hg(0)_g$  from volcanoes contributes to the global atmospheric Hg budget, co-emission of halogens (e.g., bromide) in volcanic plumes may lead to a rapid oxidation of Hg, drastically reducing Hg lifetime in the atmosphere (Lindqvist and Rodhe, 1985; Slemer et al., 1985; Lindberg et al., 2007; von Glasow, 2010). Rapid oxidation of  $Hg(0)_g$  would enhance Hg(II) deposition in the surrounding environment, after which it could be incorporated into soils and vegetation (Martin et al., 2011, 2012).

An alternative approach to direct measurements of  $Hg(0)_g$  for estimating the contribution of volcanoes to regional and global Hg is using geological archives. Amongst them, sediment cores of lakes located in volcanic settings are particularly valuable, because they enable the reconstruction of past Hg deposition and an investigation of the contribution of volcanism with regards to other geological, climatic, and anthropogenic sources by combining analyses of Hg and relevant compounds. Moreover, thanks to high sedimentation rates [e.g., between mm to m of thickness for plinian deposits (Walker, 1981)], lake sediment can record information on post-eruptive Hg deposition, in relation to the intensity and nature (effusive, explosive) of the eruption. Unfortunately, paleoenvironmental reconstructions that include Hg remain infrequent, especially in the context of volcanic eruptions (Roos-Barracough et al., 2002; Shotyk et al., 2002; Ribeiro Guevara et al., 2010; Hermanns and Biester, 2013). Thus, extrapolating the available data to estimate volcanic contributions to Hg budgets at regional and global scales is still difficult.

In the Andean belt (South America), the seismo-tectonic activity along the Southern and Austral Volcanic Zones (13–55°S) is substantial

(Thouret et al., 1999; Bertrand et al., 2008; Stern, 2008; Anselmetti et al., 2009; Sandri et al., 2014; Lahsen et al., 2015; Samaniego et al., 2016). Numerous volcanic eruptions have been recorded during the mid- and late-Holocene in geological archives (Cole-Dai et al., 2000; Ribeiro Guevara et al., 2010). In the Central Andes, concentrations of insoluble dust particles in the Nevado Sajama and the Quelccaya ice core records showed a marked increase from ca. 7500 to 3400 yr cal. BP (Thompson et al., 1998), coinciding with a recurrence of regional major explosive eruptions (Thompson et al., 1998). In particular, the sediment of the Lake Chungará (Chile) recorded a phase of enhanced volcanic activity of the Parinacota volcano, starting about 14,000 years ago (Mühlhauser et al., 1995; Valero-Garcés et al., 1996; Moreno et al., 2007; Saez et al., 2007; Giralt et al., 2008; Hernandez et al., 2008; Pueyo et al., 2011). Besides volcanic activity, the Central Andes are also known for historical mining activities. The pre-Colonial period of smelting Andean silver ores produced substantial Hg emissions as early as the twelfth century and was followed by the onset of large-scale emissions in the mid-sixteenth century (colonial period) when the Hg amalgamation process was generalized (Cooke et al., 2009; Cooke et al., 2011; Cooke et al., 2013).

In this study, millennial-long Hg deposition changes and related forcing mechanisms were investigated in sediment records of Lake Chungará (4520 m a.s.l.), northern Chile. This site, located in poorly vegetated foothills (i.e., minor terrestrial Hg pool) of the Parinacota volcano, is representative of the high-altitude central western Andean environments. Hg concentrations and accumulation rates were reconstructed at high-resolution (mm to cm scale) in a sediment sequence that covers the last 2700 years cal. BP together with inorganic geochemistry, total carbon, carbon stable isotopes ( $\delta^{13}C$ ) and organic matter (OM) molecular composition. Inorganic geochemical data (from X-Ray Fluorescence core scanner analyses) allow accurate identification of the volcanic events and associated mineral deposition, while  $\delta^{13}C$  and organic compounds (from pyrolysis-gas chromatography/mass spectrometry -Py-GC/MS- analyses) provide proxies of terrestrial and in-lake productivities (Ishiwatari et al., 1991; Tolu et al., 2015). The objective of this study is two-fold; (i) to better understand the mechanisms of Hg deposition in consideration of volcanism, lake geochemistry and ecology, and (ii) to quantitatively estimate the contribution of volcanic and anthropogenic forcing on late-Holocene Hg deposition in the Central-western Andes.

## 2. Materials and methods

### 2.1. Lake Chungará: climatic, geological and ecological settings

The Chilean Altiplano is a high-altitude plateau (average elevation of 3750 m a.s.l.) located in west-central South America. The climate is semi-arid to arid, with an average annual temperature of 4.2 °C, with large diel variation (~25 to 20 °C). Annual rainfall ranges from 345 to 394 mm (Mühlhauser et al., 1995), and has a well-defined seasonal cycle, with the rainy season between December and March. Due to its high altitude, evaporation is high and was estimated at 1200  $mm\ yr^{-1}$  (Mladinic et al., 1987).

Lake Chungará (18°15'S, 69°09'W; 4520 m a.s.l.; surface area, 22.5  $km^2$  and maximum depth, 40 m), is located in the active setting of the Parinacota volcano (6348 m a.s.l.). It was formed after a partial collapse of the earlier Parinacota stratocone, which dammed the ancient

Lauca River between 15 and 17 kyr cal. BP (Hora et al., 2007). The lake is polymeric, moderately alkaline (pH between 8.99 and 9.30), well mixed ( $7.6 \mu\text{L L}^{-1}$  O<sub>2</sub> at 34 m deep), and has a moderate salinity [ $1.3 \text{ g L}^{-1}$ ; (Risacher et al., 1999)]. Its catchment (surface area, 273 km<sup>2</sup>) is topographically closed without surface outlets (Fig. 1). Lake primary productivity is dominated by algal communities (diatoms and green algae) in the deep lake waters, whereas macrophytes are important in the littoral zone (Mühlhauser et al., 1995). The Ajoya and Parinacota volcanoes constitute the steep western and northern slopes of the lake margins, whereas the distal fringe of recent alluvial fans and the River Chungará valley form the gentle eastern and southern margins. The northern shore of Lake Chungará consists of 30–50 m thick andesite lavas [59–61% SiO<sub>2</sub>, (Clavero et al., 2004)] composed of a plagioclase-clinopyroxene-orthopyroxene-amphibole phenocryst assemblage. Due to the high altitude and arid conditions, the margins are covered by dry Puna vegetation, dominated by wiry tussock-like grasses (Baied and Wheeler, 1993) and characterized by assemblages of cushion and mat of low coverage and density (S.I.1).

During the last 4000 yr cal. BP, the climate has been characterized by relatively moist conditions compared with an arid mid-Holocene (Marchant and Hooghiemstra, 2004), which has resulted in lake-level increases in the Central Andes. This period has also been characterized by intense volcanic activity, mainly explosive, releasing large amounts of volcanic materials to the lake (Wörner et al., 2000; Clavero et al., 2002).

## 2.2. Sediment core collection

Two sediment cores were collected in the western basin of Lake Chungará at a water depth of 29.4 m, using a UWITEC gravity corer: CG02 (S 18°15.110' W 69°09.784'; length: 0.83 m) and CG03 (S 18°15.124' W 69°09.769'; length: 1.46 m). Sampling was performed in October 2014 during the late dry season. For both cores, an intact 22 mm width U-Channel sub-core was retrieved for XRF core-scanning analysis. For chronological and chemical analyses, subsamples were taken using cylindrical punches (diameter: 20 mm) on 0.5 cm-

thick sediment slices for the first 20 cm and then on 1 to 2 cm thick slices downcore (adapted to sedimentological variations). Further details about core opening, subsampling procedures, and cross-correlations are given in Supplementary information S.I.2.

## 2.3. Chemical analyses

All details for the chemical analyses are given in S.I.2 for sedimentology, in S.I.3 for Hg and X-Ray Fluorescence (XRF) analyses, and in S.I.4 for organic matter composition (Py-GC/MS), carbon content, and isotopic composition (CM-CRDS) analyses.

Briefly, XRF core scanning was performed at 1 mm steps on an Avaatech core scanner using different tube settings: at 10 kV–2 mA for Al, Si, S, K, Ca, Ti, Mn, Fe and at 30 kV–0.5 mA for Br, Sr, Rb, and Zr (Richter et al., 2006).

For each sediment subsample, water content was obtained from the difference in weight prior and post freeze-drying and then, dry bulk density (DBD) was calculated considering the subsample volume. Sediment subsamples were finely ground (<63 µm) using an agate mortar before all analysis (S.I.2).

Total mercury concentrations ([THg]) were determined by combustion and atomic absorption spectrophotometry using an AMA 254 analyzer (Altec) (Guédron et al., 2009; Guédron et al., 2011). Concentrations obtained for repeated analyses of certified international reference materials (i.e., MESS-3 of National Research Council of Canada;  $0.091 \pm 0.008 \text{ ng g}^{-1}$ ) never exceeded the certified range (S.I.3). Hg accumulation rates (HgAR) were calculated by multiplying the DBD and [THg] divided by the number of years covered by the slice.

Total carbon content (TC, %) and isotopic composition ( $\delta^{13}\text{C}$ , ‰) of bulk sediment were measured by Cavity Ring-Down Spectrometer (Picarro, Inc.®) coupled with Combustion Module (Costech, Inc.®) (CM-CRDS) using previously reported analytical methods, calibration, and sample preparation (Balslev-Clausen et al., 2013; Paul et al., 2007). Total organic carbon (TOC) and its isotopic composition ( $\delta^{13}\text{C}$ ,

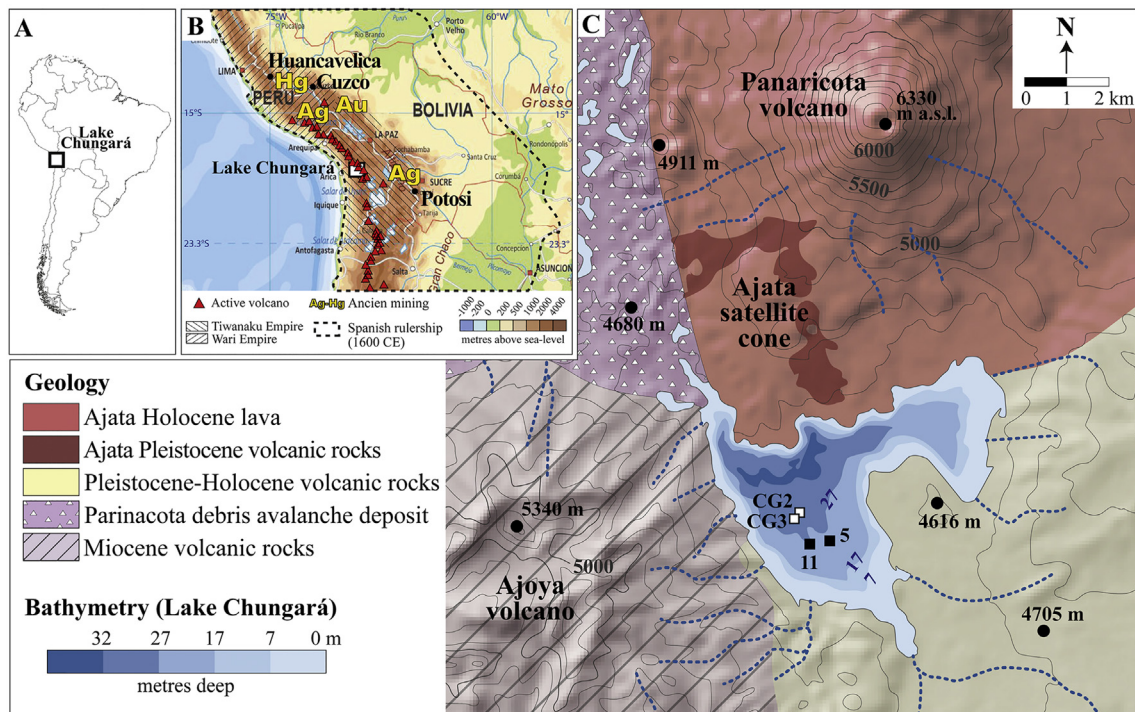


**Fig. 1.** A) Location of Lake Chungará on the South American map, B) regional active volcanoes locations, historical mining silver (Ag) and mercury (Hg) areas and Tiwanaku/Wari empire extensions [modified from Lahsen et al., 2015] and C) geological and topographical map of the studied area [modified from Saez et al., 2007 and Pueyo et al., 2011] and bathymetric map of Lake Chungará with sampling locations for cores CG02 and CG03 (this study) and cores 5 (Moreno et al., 2007) and 11 (Saez et al., 2007).

%) were also determined after removal of the carbonates via aqueous acidification (SI.4a) on a sub-set of sediment samples ( $N = 20$ ; Fig. S4).

Organic matter composition was determined by pyrolysis (PY-2020iD and AS-1020E, FrontierLabs, Japan) – gas chromatography/mass spectrometry (Agilent, 7890A-5975C, Agilent Technologies AB, Sweden) following the method developed by Tolu et al. (2015). Except for a few samples taken within tephra layers where no data could have been obtained, 99 pyrolytic organic compounds were identified belonging to 9 classes of OM (i.e., carbohydrates, N-compounds, (poly)aromatics, phenols and lignin oligomers, *n*-alkenes, *n*-alkanes, alkan-2-ones, and chlorophyll). A detailed list providing information on the molecular mass and structure, and the references for mass spectra is provided in SI.4. (Table S1). For each identified organic compound, relative abundances were calculated by setting the sum of peak areas of identified organic compounds to 100%; the peak areas (i.e., signal intensity) of each pyrolytic organic compounds is proportional to the concentration of the organic compounds the pyrolytic compounds derive from (SI.4.c).

#### 2.4. Chronology

Short-lived radionuclides ( $^{210}\text{Pb}$  and  $^{137}\text{Cs}$ ) were analyzed at an interval of 0.5 cm over the uppermost 10 cm of the CG02 core, using well-type, germanium detectors at the Laboratoire Souterrain de Modane (France) and following the procedure of Reyss et al. (1995).

Gastropod shells from sediment slices were cleaned by sonication in ultrapure water. Seventeen samples were dated for radiocarbon at the National Ocean Science Accelerator Mass Spectrometry (USA) on a 500 kV Pelletron AMS device (SI.5). Radiocarbon ages were calibrated to calendar years Before Present (cal. yr BP) using the SHCal13 calibration (Hogg et al., 2013) and post-bomb curves (Hua et al., 2013). The age-depth model was built using the 'clam' R package (Blaauw, 2010). Details for construction of the age–depth model are given in SI.5 and Fig. S7.

### 3. Results and discussion

#### 3.1. A 2700 years calendar of the Parinacota eruptions

The chronology of Parinacota eruptions was established through the combination of short-lived radionuclides ( $^{210}\text{Pb}$  and  $^{137}\text{Cs}$ ) and 17 radiocarbon ages (Table S4). The constant flux constant sedimentation rate (CFCS) model applied to the  $^{210}\text{Pb}_{\text{ex}}$  activities (Golberg, 1963) yielded a mean accumulation rate of  $0.95 \pm 0.04 \text{ mm yr}^{-1}$  ( $1\sigma$ ) over the top 10 cm that is in good agreement with  $^{137}\text{Cs}$  data (Fig. S7A). Cross-dating between the short-lived radionuclides model and one  $^{14}\text{C}$  age (Sabatier et al., 2010) obtained on a gastropod shell collected at 6 cm depth in the same core indicated a lake water reservoir age of  $4140 \pm 30$  yrs. This value is 880 years higher than the one obtained by dating modern dissolved inorganic carbon (Giralt et al., 2008). Even if the lake-water reservoir effect may have changed, mostly because of hydrothermal volcanic activity, independent radiocarbon dating of the Parinacota lava deposits matched well with the proposed tephra chronostratigraphy (Fig. S7B), supporting our lake-water reservoir age estimate of  $4140 \pm 30$  yr for the study period. Altogether, the sediment sequence covered the last 2900–2400 years (2 $\sigma$  interval). The calculated mean sedimentation rate was  $0.30 \pm 0.7 \text{ mm yr}^{-1}$  from 2700 to 1400 yr cal. BP and  $0.48 \pm 0.5 \text{ mm yr}^{-1}$  from 1400 cal. yr BP to present.

Cores CG02 and CG03 were collected in the deepest area of the lake that was reported to record the maximum pyroclastic fallout [(Moreno et al., 2007; Saez et al., 2007) – Fig. 1]. Based on lithological and geochemical composition, the core CG03 was divided into 3 units; the first one from the surface to 18.5 cm (i.e., 300 yr cal. BP to present); the second one from 18.5 to 108 cm (i.e., 1400 to 300 yr cal. BP); and the third one from 108 to 146.5 cm (i.e., 2700 to 1400 yr cal. BP). In total, 20 volcaniclastic layers (tephras) were identified based on increases in DBD and major elements (e.g., K, Fe, and Al, mirrored by drops in TC content – Fig. 2), which reflect rapid deposition of dense

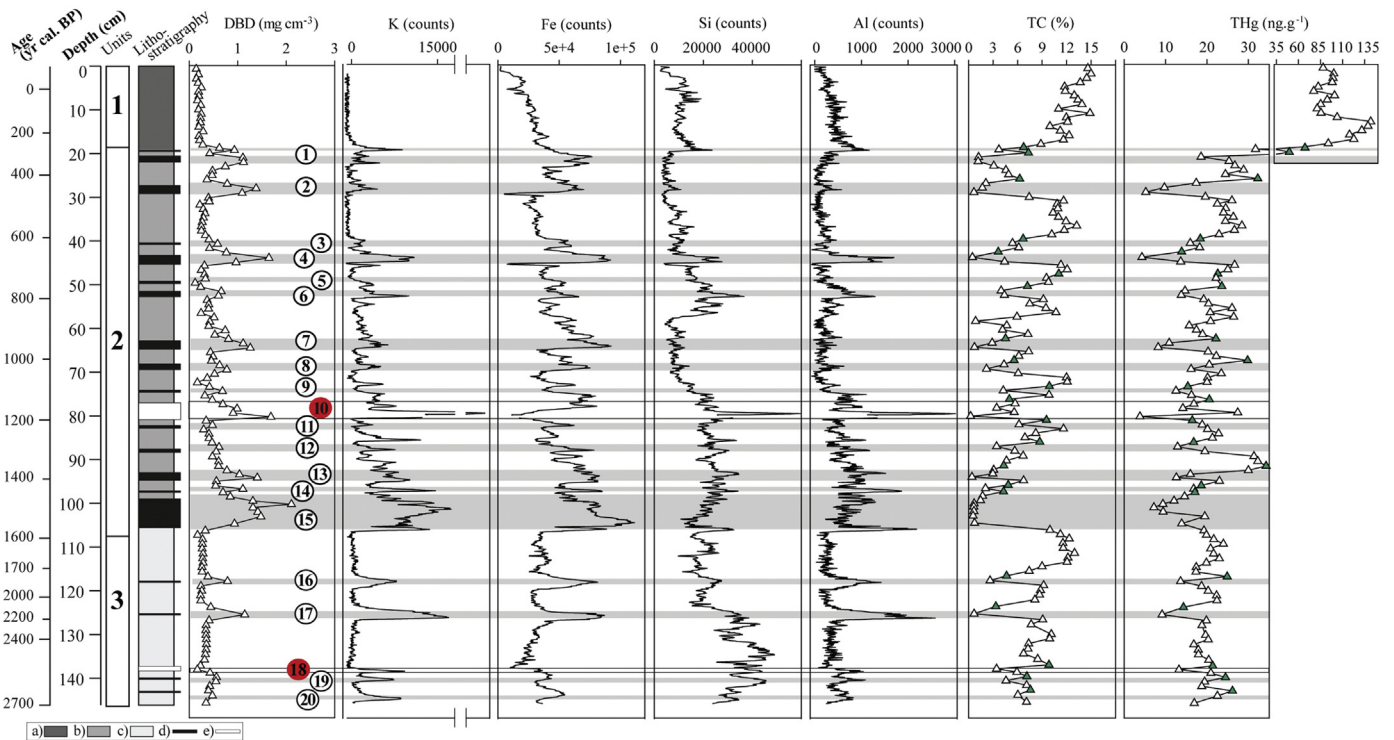


**Fig. 2.** Depth and age profiles of (i) dry bulk density (DBD), (ii) XRF-signals (counts) of K, Fe, Si, and Al, (iii) total carbon content (TC) and (iv) total mercury content (THg) for the core CG03. All volcaniclastic layers (tephras) are numbered in the left panel. Dark mafic volcaniclastic layers correspond to gray bands with numbers in white circles, and white rhyolitic volcaniclastic layers correspond to white bands with numbers in red circles. Post-deposition Hg peaks are colored green. Lithostratigraphy: a) black homogeneous diatom-gyttja, b) black to green diatom-gyttja, c) black to brown diatom-gyttja, d) dark mafic tephra layer, e) white rhyolitic tephra layer.

materials impoverished in organic matter and rich in volcaniclastic minerals (Giralt et al., 2008). Unit 2 had the highest density of tephras (i.e., 15 layers between 1400 and 400 yr cal. BP) compared to unit 3 (5 layers between 2700 and 1400 yr cal. BP). No volcanic depositions were identified in unit 1. Two different types of tephra layers were distinguished: (i) 18 dark mafic layers enriched in K, Fe, Al, Ti, Rb, and Zr and depleted in Si and Ca; and (ii) two white rhyolitic layers enriched in Si and K and impoverished in Fe, Ti, Zr, Ca, and Sr (S.I. 3, Figs. S2 and S3). These latter displayed higher  $\delta^{13}\text{C}$  values, suggesting a significant relative contribution of carbonates [i.e., positive  $\delta^{13}\text{C}$  values (Pueyo et al., 2011)] relative to organic carbon and thus indicating materials coming from the crust as compared to the dark mafic materials originating from the mantle (Figs. 3 and S4).

In-between the tephra layers, volcaniclastic tracers (DBD and geochemical tracers) returned to baseline values within a few millimeters above the tephra layers, except for the events numbered 2, 7, 10, and 15. This suggests that catchment leaching of fresh volcaniclastic deposits to the lake was fast and likely restricted to short periods. This short-term transfer can be explained by (i) the steep slopes of the stratocone with scarce vegetation cover that is unfavorable to material retention in the lake catchment; (ii) the low amount of precipitation that limits the remobilization of this material; and (iii) the abundant macrophytes in the shallow littoral zone acting as a physical barrier (Saez et al., 2007). The events 2, 7, 10, and 15 that displayed a slower return of volcaniclastic tracers to baseline values ( $>1$  cm), seem to have been more intense than the other volcanic eruptions given the higher

thickness of their tephra layers and the higher intensity of their increases in DBD and/or geochemical tracers (Fig. 2). However, evaluating the amplitude of each volcanic event is difficult, because deposition of volcanic ash can show a highly variable spatial distribution mostly due to the dynamics of dominant winds and lake surface currents (Saez et al., 2007; Daga et al., 2008).

### 3.2. Impact of volcanic eruptions and climate change on the lake ecosystem

#### 3.2.1. Evidence for changes in aquatic and terrestrial productivity

Outside of the volcaniclastic events, the  $\delta^{13}\text{C}$  values of bulk sediment (from  $-19$  to  $-14\text{\textperthousand}$  – Figs. 3 and 4) were in the reported range for algae (diatom, green and brown algae) and/or macrophytes (e.g., Characeæ) found in Lake Chungará (Pueyo et al., 2011). In addition, lignin oligomers [a specific proxy for higher plants (Meyers and Ishiwatari, 1993)] always occurred at low levels, whereas the ratio of N-compounds to carbohydrates [a proxy for algal vs plant OM (Bianchi and Canuel, 2011)] was high compared to sediment from boreal lakes [S.I.4, Table S3 – (Ninné et al., 2017; Tolu et al., 2017)]. Both independent tracers confirm the hypothesis made by Pueyo et al. (2011) based on the carbon:nitrogen ratio (C/N), on the dominance of algal OM as a source of organic matter (OM) for offshore sediment.

For the entire CG03 core, TC mirrored the distribution of volcaniclastic material tracers (DBD and K – Fig. 2), indicating a strong decline in the sediment OM content during and immediately after volcanic eruptions that can be ascribed to dilution by massive deposition

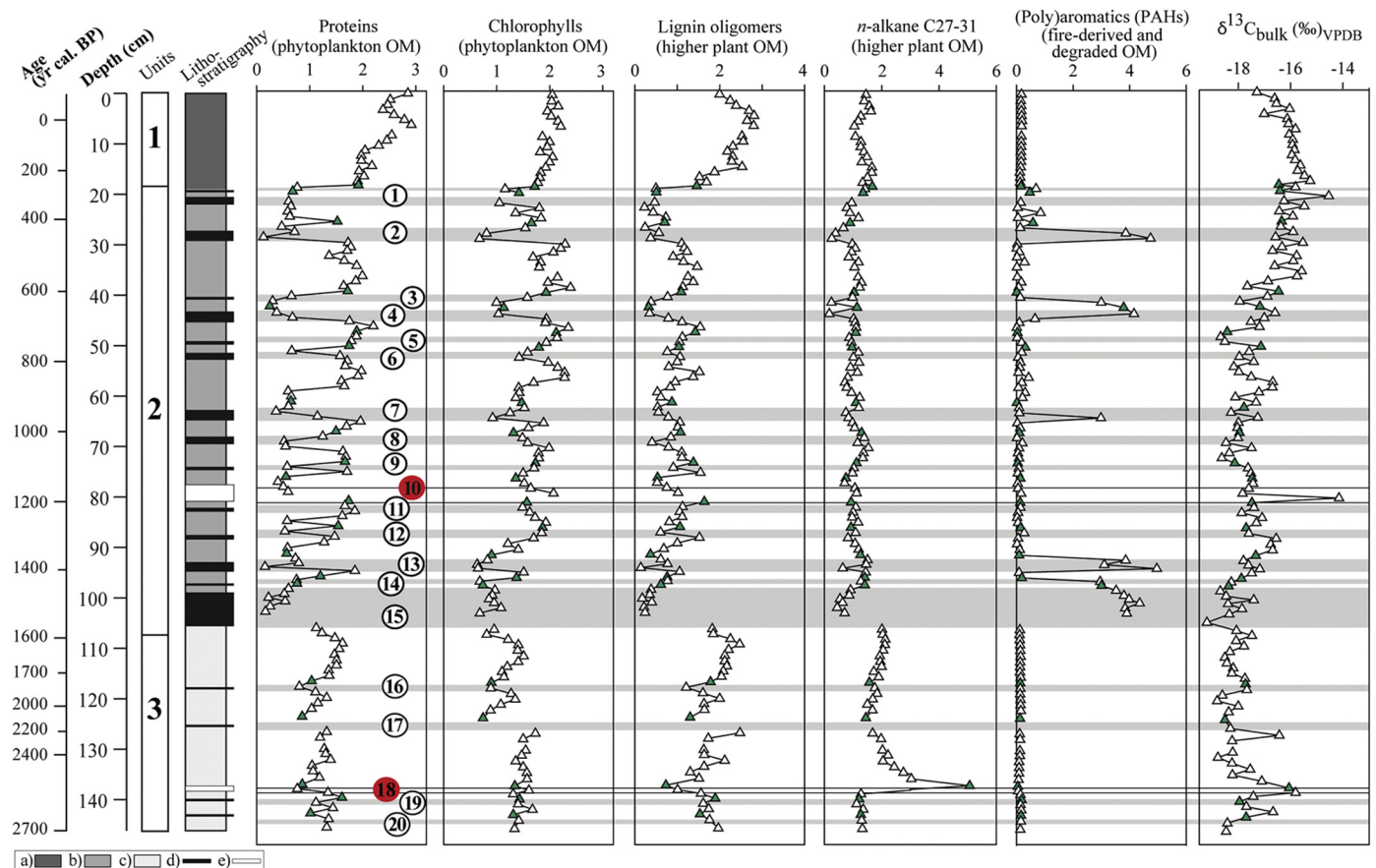


**Fig. 3.** Depth and age profiles of (from left to right) (i) the abundance of biomarkers of algal organic matter (i.e., proteins and chlorophylls), (ii) the abundance of biomarkers of higher plants (lignin oligomers and n-alkanes C27–31), (iii) the abundance of polyaromatic compounds (PAHs), an indicator of fire events and degraded OM, and (iv) carbon stable isotope signature of bulk sediment ( $\delta^{13}\text{C}$ ) for the core CG03. Missing biomarker data in profiles correspond to insufficient carbon content for Py-GC/MS quantification. All volcaniclastic layers (tephras) are numbered in the left panel. Dark mafic volcaniclastic layers correspond to gray bands with numbers in white circles, and white rhyolitic volcaniclastic layers correspond to white bands with numbers in red circles. Post-deposition data are colored green. Lithostratigraphy: a) black homogeneous diatom-gyttja, b) black to green diatom-gyttja, c) black to brown diatom-gyttja, d) dark mafic tephra layer, e) white rhyolitic tephra layer.

of inorganic material. While  $\delta^{13}\text{C}$  did not always show consistent trends with respect to volcanic events (Fig. 3), the relative abundances of various organic compounds indicated substantial changes in primary productivity (Fig. 3 and S.I.4). To assess changes in OM sources and biological activities, relative abundances were used instead of the semi-quantitative peak area dataset due to the strong dependence of this latter on TC variations (see S.I.4.c for detailed explanations). Most of the volcanic events (i.e., 16 out of 20; numbered 1–4, 6–10, 12–13, and 15–19) were associated with declines in the abundance of proteins [identified from their specific pyrolytic products, 2,5-diketopiperazines (Fabbri et al., 2012)] and/or of chlorophyll [identified from their specific pyrolytic products, prist-1-ene and phytadienes; (Ishiwatari et al., 1991)]. Both, proteins and chlorophyll are typically found in larger quantities in algae than in plants, the plants being instead richer in carbohydrates and polysaccharides (Bianchi and Canuel, 2011). Moreover, the relative abundances or contents of proteins and chlorophyll in sediment have been shown to be good proxies of algal production when determined by Py-GC/MS (Peulvé et al., 1996; Ninnis et al., 2017; Tolu et al., 2017) or other methods (Michelutti et al., 2005; Ady and Patoine, 2016). While the abundances of proteins and chlorophyll declined, the abundance of (alkyl)pyrroles, which are indicators of degradation products of proteins, chlorophylls, and other aquatic organism N-compounds (Damsté et al., 1992; Jokic et al., 2004; Schellekens et al., 2009; Tolu et al., 2017), remained stable or increased (S.I.4., Fig. S6). These results suggest death of aquatic organisms and the degradation of their organic residues during volcanic eruptions, due to multiple factors, such as a decrease in water column transparency, an increase of lake surface-water temperature, and a decrease in pH resulting from the heat and volatiles emitted (Ohba et al., 1994; Pasternack and Varekamp, 1997; Varekamp et al., 2000; Stewart et al., 2006). Accumulations of bivalve shells at the base of several fine tephra layers were also observed and can be interpreted as 'obrution' deposits caused by their sudden death and burial under massive inorganic inputs (Brett, 1990). Releases of hydrothermal fluids during eruptions, which are known to cause changes in the water physico-chemistry and thus modifications in biota assemblages, have also to be considered (Valero-Garcés et al., 1999; Giralt et al., 2008).

### 3.2.2. Evidence for wildfires and biotic recovery following eruptions

The sixteen volcanic events showing a decline in aquatic productivity, with the exception of the 6th, also exhibited declines in the abundances of lignin oligomers and straight *n*-alkanes with 27 to 31 carbons (Fig. 3), which are two proxies for plant OM inputs (Meyers and Ishiwatari, 1993; Bush and McInerney, 2013). Similar to lignin oligomers and straight *n*-alkanes C27–31, the abundances of specific pyrolytic products of polysaccharides (i.e., levosugars, 4-hydroxy-5,6-dihydro(2H)-pyran-2-one, dianhydrorhamnose and maltol), known to be in higher abundance in higher plants vs algae, also strongly decreased (S.I.4., Fig. S6). These declines in plant OM inputs indicate a reduction, during and immediately after volcanic eruptions, of terrestrial OM inputs to the lake and/or of terrestrial plant productivity due to, respectively, burial of the terrestrial OM pool by volcaniclastic materials and/or wildfires. This latter suggestion is corroborated for the volcanic events numbered 1, 2, 4, 7, 13, 14 and 15, for which strong increases were observed in the abundances of the three identified polycyclic aromatic hydrocarbons (PAHs; Fig. 3), i.e., two methyl-indenes and a methyl-naphthalene (Table S1). Such polycyclic aromatic hydrocarbons have been identified as major products of black carbon (Kaal et al., 2009) and have been used as indicators of fire in peat archives and natural waters (Schellekens et al., 2009; Kaal et al., 2016). Following each deposition of volcaniclastic materials, the abundances of proteins and chlorophyll, as well as lignin oligomers and *n*-alkanes C27–31, gradually increased, indicating that the aquatic biota and the terrestrial vegetation or the inputs of terrestrial OM pool gradually recovered from the volcanic eruptions (Fig. 3).

### 3.2.3. Evidence for a climate change response of the lake and catchment ecosystem

Insignificant differences between total carbon or  $\delta^{13}\text{C}$  values obtained on bulk vs decarbonated samples (Fig. S4) confirm previous studies indicating that the inorganic carbon fraction in sediment from the deeper area of Lake Chungará deposited after 2700 yr cal. BP (i.e., same time interval than in this study) is not significant [ $\sim 1\%$ ; (Moreno et al., 2007; Saez et al., 2007; Pueyo et al., 2011; Bao et al., 2015)]. Therefore, the  $\delta^{13}\text{C}$  values in bulk sediment are representative of the OM signature and the  $\sim 5\%$  range of variation is likely due to changes in aquatic productivity [i.e., changes in benthic vs planktonic activity; (Bao et al., 2015)] and/or changes in allochthonous (i.e., terrestrial) inputs, most probably in response to climate change over the last 2700 years. It is worth pointing out that in unit 2, the numerous volcanic events in a short timeframe (i.e., 15 tephras in  $\sim 1000$  years) may cloud the signal of biomarkers and climate proxies; that is, lake recovery from a volcanic eruption might not be reached completely before the next eruption. However, except for the cases of identified wildfires, the entire set of biomarkers returned to baseline values immediately after each tephra.

Considering the continuous sedimentation period (i.e., excluding tephras; Fig. 4C), the entire unit 3 and the first half of unit 2 had amongst the lowest average  $\delta^{13}\text{C}$  values (i.e.,  $-17.8 \pm 0.6\text{\textperthousand}$ ) of the record, except a marked increase at the transition between unit 2 and 3 (i.e., after tephra 15;  $-17.0 \pm 0.4\text{\textperthousand}$ ). This latter interval together with the following second half of unit 2 exhibited a rise to approximately  $-16.5\text{\textperthousand}$ , indicating an higher contribution of aquatic productivity (algae and macrophytes) with respect to terrestrial OM inputs, likely resulting from a wetter climate and a rise in lake-level compared to the previous period. This trend continued and was accentuated in the following unit 1, with the highest average  $\delta^{13}\text{C}$  value (around  $-15.5\text{\textperthousand}$ ). In contrast, from 10 cm to the core surface,  $\delta^{13}\text{C}$  strongly decreased to approximately  $-18\text{\textperthousand}$ , possibly due to (i) an increased contribution of terrestrial OM via run-off (Cole et al., 2011) that is also supported by the increases in carbohydrates and lignin oligomers, and (ii) a lower pelagic-benthic production coupling due to the possible stratification of the lake (Bao et al., 2015). It may also result from the global and progressive decrease of the atmospheric  $\delta^{13}\text{C}$   $\text{CO}_2$  value [Suess effect (Verburg, 2007)] since the beginning of the industrial era (around 1870 CE, i.e. 80 yr cal. BP, Fig. S10B) due to the combustion of fossil fuels depleted in  $^{13}\text{C}$  as recorded in recent sediment (Körtzinger et al., 2003; Hellevang and Aagaard, 2015).

Throughout the entire sequence, decadal to centennial variations in  $\delta^{13}\text{C}$  can also be the fingerprint of changes in algal and microbial communities (Bade et al., 2006; Dorador et al., 2013; Vuillemin et al., 2017; Aguilar et al., 2018). Indeed, climate changes, especially in temperature, can impact the communities and metabolism of microorganisms (Kraemer et al., 2017), although it is sometimes difficult to differentiate autochthonous from allochthonous OM supply, because  $\delta^{13}\text{C}$  from algal and terrestrial OM can be similar in some cases (France, 1997; Cole et al., 2011). Nevertheless, OM biomarkers indicate that, while substantive terrestrial inputs cannot be completely ruled out, algal OM was the dominant C component of CG03 sediment; indeed, the coring site was located in the off-shore part of the lake, compared with littoral areas containing larger amounts of macrophytes (Apolinarska et al., 2011).

### 3.3. Mechanisms of Hg deposition (following volcanic eruptions) and incorporation in sediment

The layers of massive inorganic volcaniclastic deposits (tephras) had the lowest Hg concentrations ([THg] from 4 to  $13\text{ ng g}^{-1}$ ), similarly to other sediment archives retrieved in volcanic settings (Biester et al., 2002; Ribeiro Guevara et al., 2010; Daga et al., 2016). These low values were, in most cases, followed by sudden increases in [THg], up to  $32\text{ ng g}^{-1}$ , i.e., within the next 1–2 cm sediment layer (green symbols in Fig. 2), especially after the events n° 1–2, 4, 6, 7, 8, 10, 13, 16 and 17. It is noteworthy that these [THg] patterns were similar for both

the white rhyolitic (crustal volcaniclastic materials) and the dark mafic (mantle volcaniclastic materials) tephras (cf. Sub-section 3.1), suggesting that Hg deposition was similar for the two types of volcanic events. Post-tephra Hg peaks were previously reported in Patagonian sediment records and were attributed to the transfer and deposition of Hg contained in terrestrial biomass following wildfires in the catchment, resulting from natural or human-induced forest fires or occurring naturally together with volcanic events (Ribeiro Guevara et al., 2010; Daga et al., 2016). This explanation does not seem to hold true in the case of Chungará, because increases in the abundance of PAHs were only found for a few of the 20 recorded volcanic eruption events (Section 3.2.2) and were not synchronous with the sudden increases in Hg concentrations after the tephra deposition (Fig. 3). The Chungará catchment is only sparsely covered with grassland vegetation (Section 2.1 and S.I. 1), which likely represents a minor pool of Hg. The diagenetic upward remobilization of Hg from the OM-depleted tephra layers could have contributed to such post-tephra Hg peaks. However, only few studies have found evidence of Hg remobilization in sediment, resulting from the degradation of OM and dissolution of authigenic Fe-oxides, and later scavenged by OM and/or authigenic sulfides in upward sediment layers (Gobeil and Cossa, 1993; Rydberg et al., 2008; Mucci et al., 2015). In support of limited or non-existent Hg mobility, there was neither systematic nor synchronous increases in Fe, Mn, or S with Hg in the above tephra layers (S.I. 6). Hence, both wildfires and diagenetic remobilization are not the most likely mechanisms to explain the post-tephra Hg peaks observed.

The most plausible explanation for these post-tephra Hg peaks is a decrease in sedimentation rate after volcanic eruptions together with a constant or increased Hg deposition. A decline in aquatic productivity was found for almost all volcanic events (Section 3.2.2.) that may lead to decrease in sedimentation rate (decrease of organic material inputs) after the tephra deposit. In the meantime, atmospheric Hg deposition likely increased after the coarse tephra deposition resulting from dry (i.e., Hg associated with fine volcaniclastic particles) and wet (i.e., precipitation) deposition of Hg (directly to the lake or mobilized from the catchment; Section 3.1). The deposition of gaseous Hg(0)<sub>g</sub> emitted during the eruption may have been a significant source of Hg(II) to the lake after possible atmospheric oxidation by co-emitted halogens [e.g., Br - Fig. S3 (von Glasow, 2010; Bagnato et al., 2014)]. Once in the lake, Hg(II) would be redistributed together with particulate natural organic matter or algae, which, respectively bind and sorb Hg(II) (Loux, 1998; Soto Cardenas et al., 2018). Both fine particles and natural organic matter are characterized by sedimentation rates (much) lower than the coarse volcaniclastic materials. Although the [THg] and TC profiles were overall similar, the post-tephra Hg peaks coincided neither with increases in TC nor increases in the abundances of organic biomarkers for fresh algal and plant OM, as these parameters mostly increased gradually following the tephras (Figs. 2 and 3; Section 3.2.2).

In the sections of the sediment sequence with uninterrupted lake-sediment deposition (i.e., excluding the tephra deposits), algae may represent a substantial pool of Hg in the sediment. The efficiency of Hg scavenging by primary producers leading to further Hg accumulation in sediment did not seem to be affected by climate change during the interval studied, because HgAR did not show significant covariations with organic biomarkers or climate proxies (see following Section 3.4). These results suggest that the total pool of organic matter in the lake was not a limiting factor for Hg adsorption [Hg concentrations in water are generally low in such high-altitude lakes (Hermanns et al., 2013; Guédron et al., 2017)] and incorporation into the lake sediment.

### 3.4. Chronology of Hg deposition: deciphering volcanic and anthropogenic contributions

The identified drivers of Hg accumulation that are of major relevance for this record are respectively (i) volcanism, (ii) anthropogenic

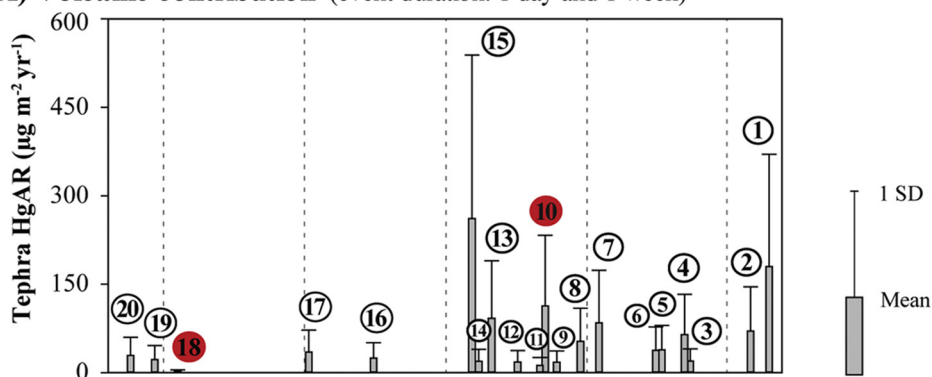
emissions and subsequent deposition, and (iii) climate change that can influence both in-lake productivity and terrestrial inputs to the lake.

The calculation of HgAR for each volcaniclastic deposition event is not straightforward, due to the complexity of estimating the duration of an event. The most reasonable duration for an explosive volcanic eruption and the deposition of a tephra ranges between a day and one week (Walker, 1981). In order to compare HgAR originating from the recorded volcanic eruptions to the one of continuous deposition, HgAR were calculated for each tephra averaged over the entire tephra thickness. HgAR varied between 1 and 475  $\mu\text{g m}^{-2} \text{yr}^{-1}$  for the 20 recorded events (Fig. 4A). The highest values were at least 2 orders of magnitude higher than the background HgAR calculated in-between the tephras (1 to 3  $\mu\text{g m}^{-2} \text{yr}^{-1}$ , Fig. 4A). Such a comparison between tephra events and average annual Hg accumulation is likely an overestimate, because each 1-cm slice of uninterrupted lake sediment deposition (i.e., in-between tephras) covered from 10 up to 40 years, which is approximately 3 orders of magnitude higher than the typical duration of a tephra deposit. To apportion the overall contribution of volcanic eruptions relative to other sources (i.e., natural and anthropogenic Hg sources) in the total inventory of Hg accumulated in the Lake Chungará without consideration of the duration of volcanic events, a mass balance of Hg accumulated per unit surface area ( $[\text{Hg}] * \text{DBD} * \text{slice thickness}$ ) was calculated considering the entire set of tephras vs the continuous organic sediment sections for the master core. From this calculation, ~32% of the total Hg inventory accumulated during the past 2700 yr was estimated to be deposited during volcanic events, ~28% derived from non-volcanic natural deposition (i.e., atmospheric and detrital) and ~40% derived from anthropogenic sources. The anthropogenic sources include 28% of the total Hg inventory from Tiwanaku/Wari and colonial mining and 12% from the Industrial revolution period (Table S5 and S.I.7 for calculation details).

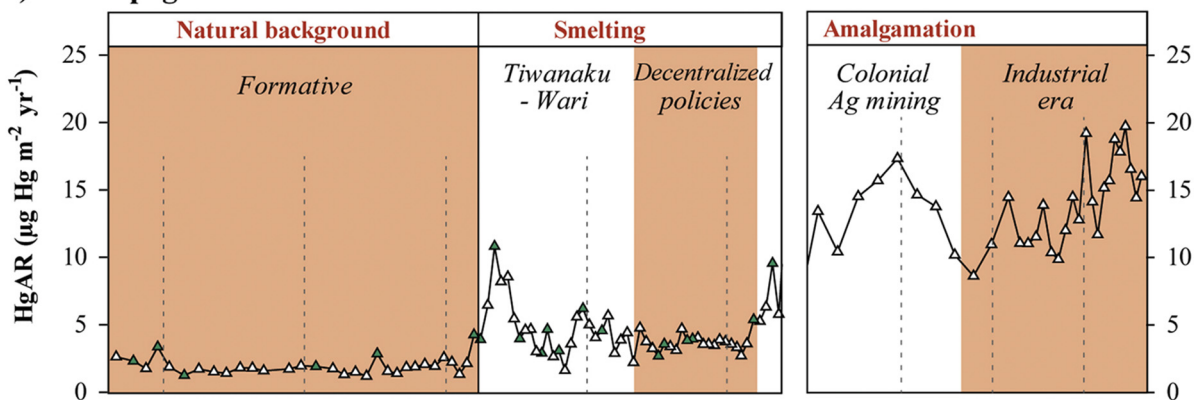
To identify the relative contribution of anthropogenic Hg emissions from the natural background, the calculated HgAR in the master core (Section 2.5 and S.I.5) during the last past 2700 years were plotted without the contribution of tephras (Fig. 4, panel B). It is worth pointing out that this plot includes post-tephra Hg deposition (green symbols in Fig. 4B) found above several tephras (Section 3.3). As previously discussed, these post-tephra increases in HgAR likely resulted from both a decrease in sedimentation rate together with a possible increase in Hg deposition to the lake, both depending on the intensity and impact of the event on the lake ecology. Hence, values obtained for post tephra HgAR might be an overestimate because a decrease in sedimentation was not considered in the age model. In the first part of the record (unit 3), HgAR ( $1.9 \pm 0.5 \mu\text{g m}^{-2} \text{yr}^{-1}$ ) was comparable to the geochemical Hg background reported for several sites in South America (Cooke et al., 2009; Cooke et al., 2013; Guédron et al., 2018b). Amongst the 5 recorded tephras in this period, only two post-tephra increases in HgAR [following the event numbered 19 ( $3.4 \mu\text{g m}^{-2} \text{yr}^{-1}$ ) and 16 ( $2.9 \mu\text{g m}^{-2} \text{yr}^{-1}$ )] exhibited higher values with respect to this background. During the following period, the highest post-tephra HgAR values were found after the most intense events (n° 1, 2, 7, 8, 10, 13 and 15) highlighting a possible relationship between post-tephra HgAR and the intensity of the volcanic event. In addition, although some of these events were encountered during periods of anthropogenic mining (n° 1, 8, 13 and 15), these increases were still identifiable suggesting that the volcanic Hg signal added to the ambient Hg level.

The relatively pristine epoch (i.e., formative period) between 2700 and 1400 yr cal. BP was followed by the first important mining era in South America, when the Tiwanaku and Wari civilizations (1500 to 850 yr cal. BP), then the colonial era (400 to 100 yr cal. BP) contributed to significant Hg inputs at a regional scale (Cooke et al., 2013; Cooke and Bindler, 2015). These mining Hg emissions were well-recorded in the Chungará sediment archive due to the western down-wind position of the lake (Guédron et al., 2018b). During the Tiwanaku and Wari epoch, HgAR increased up to  $10.8 \mu\text{g m}^{-2} \text{yr}^{-1}$ , likely resulting from the release of Hg contained in Cu, Ag and Au ores (Cooke et al., 2011)

### A) Volcanic contribution (event duration: 1 day and 1 week)



### B) Anthropogenic contribution



### C) Influence of climate change (wet and dry periods)

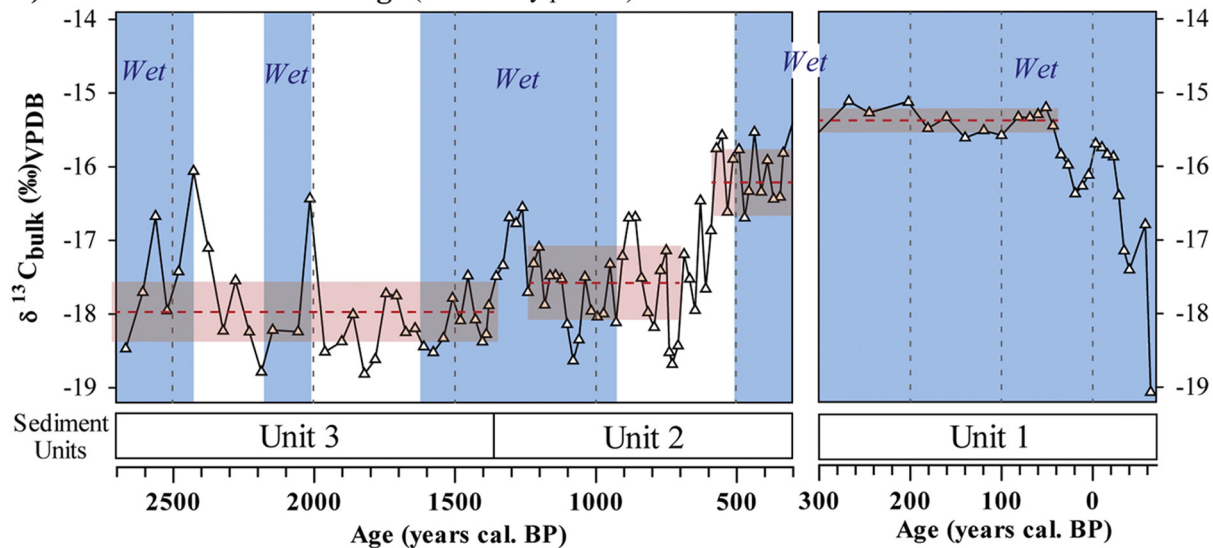


**Fig. 4.** Variability of proxies related to Hg emissions during the last 2700 yr cal. BP in the Chungará MCD sediment core. From top to bottom right: (A) calculated mean  $\pm$  1 SD Hg accumulation rates (HgAR) for each tephra\* averaged over the entire tephra thickness with an estimated durations of 1 day to 1 week (min-max), (B) calculated HgAR for continuous deposition (without tephras), including post-tephra deposits (dark green symbols) with historical periods of known mining and industrial activities, and (C)  $\delta^{13}\text{C}$  values of bulk sediment (similar to total organic carbon). Indicated on the figures are: the numbered tephras (panel A); the main techniques used in historical mining activities (panel B)\*\*; and wet (blue bands) and dry (white bands) periods (panel C) identified in Lake Titicaca records (Abbott et al., 1997; Weide et al., 2017). \*Dark mafic tephras are numbered in white circles, and white rhyolitic tephras in red circles. \*\*Note that for the colonial mining era (i.e., mostly silver mining in the Potosí area), both smelting and amalgamation were used with a dominance of amalgamation after ~200 year cal. BP.

that were smelted in numerous small metallurgical centers over the Andean Altiplano [i.e., current northern Chile and Argentina; Potosí and Lake Titicaca region in Bolivia - Fig. 1 (Lechtman, 2003; Lechtman and Macfarlane, 2005; Cruz and Vacher, 2008; Lechtman, 2014)]. The following last 400 years showed the highest HgAR values ranging from 5 to 20  $\mu\text{g m}^{-2} \text{yr}^{-1}$  (mean =  $13.1 \pm 3.6 \mu\text{g m}^{-2} \text{yr}^{-1}$ ), which is almost

7 times higher than the HgAR baseline of the formative period. During the colonial epoch, the HgAR ( $11.2 \pm 4.0 \mu\text{g m}^{-2} \text{yr}^{-1}$ ) was amongst the highest values. This period is known for the most intense historical Ag mining activities (e.g., Potosí mine) in which the Ag ores were extracted by smelting and amalgamation with elemental Hg, resulting in the largest reported historical Hg contamination in the Andes [Fig. S9

(Cooke et al., 2011; Guerrero, 2012)]. Although the extraction of Hg in the Huancavelica mine (Peru) increased until the end of the 19th century (Nriagu, 1994) to supply the mining area of Potosí, HgAR showed a decline during the 18th century that is attributable to improved extraction of Ag by Hg amalgamation, which lowered elemental Hg loss during refining (compared to smelting) through the formation of calomel, and to the improvement in the recycling of Hg during the heating stage of the amalgam [i.e., capellina (Van Buren and Cohen, 2010; Guerrero, 2012)].

This period was followed by the global industrial revolution, reported to have significantly increased atmospheric Hg emissions at the global scale (Thevenon et al., 2011; Amos et al., 2015). During this period, HgAR increased gradually from ~9 to 20  $\mu\text{g m}^{-2} \text{yr}^{-1}$  with an average value of  $14.2 \pm 3.0 \mu\text{g m}^{-2} \text{yr}^{-1}$ . This is 3 to 10 times lower than the HgAR increase recorded in sediment archives from the northern hemisphere for the same period (Thevenon et al., 2011; Engstrom et al., 2014; Cooke and Bindler, 2015; Guédron et al., 2016) and consistent with South-American archives (Lacerda et al., 1999; Biester et al., 2002; Lacerda et al., 2017). Differences between hemispheres were already indicated by atmospheric measurements and were attributed to the presence of major anthropogenic sources in the northern hemisphere coupled with a mean tropospheric residence time of total gaseous Hg of ~1 year, which does not allow complete inter-hemispheric homogenization of atmospheric Hg (Fitzgerald et al., 1983; Slemr et al., 1985; Howard et al., 2017). The comparison between these two most recent periods strikingly shows that the industrial era was of similar magnitude as the largest regional Hg contamination during the colonial mining epoch, when over 260,000 tons of Hg were used for gold and silver mining (Slemr et al., 1985; Lacerda, 1997).

Lastly, due to its high altitude (4520 m a.s.l.) at a latitude of 18°S, Lake Chungará has been subject to several paleoenvironmental changes over the approximately 2700 years covered by the record (Pueyo et al., 2011; Bao et al., 2015). During established wet and dry periods, the lake water-level has changed as well as its geochemistry (e.g., salinity) and ecological composition (Saez et al., 2007; Pueyo et al., 2011). In order to determine whether there is any imprint on the Hg record in response to past climate changes, the Hg record was compared to proxies of wetter and drier conditions in Lake Chungará record, i.e. the  $\delta^{13}\text{C}$ , TC, and organic biomarkers (Section 3.2.3 and Fig. 4) whose patterns of variation were consistent with prior paleoclimatic records of Lakes Chungará (Pueyo et al., 2011) and Titicaca (Abbott et al., 1997; Weide et al., 2017). In unit 3 of the Chungará record that is unaffected by mining activities, the profile of HgAR did not exhibit an overall co-variation with  $\delta^{13}\text{C}$  or organic biomarkers (Fig. 4, Panel C) suggesting that centennial-scale climate changes did not significantly modify Hg incorporation to the sediment. This observation confirms the previous discussion (Section 3.3) emphasizing that primary production was not restrictive for Hg adsorption and incorporation into Lake Chungará sediment. It also supports the interpretation that long-term changes in aquatic productivity did not affect HgAR through an increase of the biological pump during periods of higher productivity as proposed in a recent study (Biester et al., 2017). In addition, HgAR remained stable during this entire unit, although 5 tephras were recorded suggesting that lake ecosystem resiliency after volcanic eruptions was short enough to not affect HgAR at the resolution of the record. In the following period, i.e., between 1400 and 900 yr cal. BP (unit 2), the higher frequency of volcanic events (including the most intense events and wildfire episodes) interrupting the record make an analysis of the influence of climate changes on the Hg record more difficult (see Section 3.2.3). Finally, from the onset of industrialization, lake sediment recorded global anthropogenic emissions.

Based on this millennial-long perspective, anthropogenic and volcanic sources will likely remain the main drivers of Hg deposition in the high altitude Andes rather than modern climate warming and its local effect on the hydrological balance (Rabatel et al., 2013) and the ecosystems (Zimmer et al., 2017). Still, local and regional studies of natural archives along spatial gradients from volcanic sources are needed to

estimate the area impacted by such events, considering the influence of dominant winds.

#### 4. Conclusion

Due to its remote high-altitude location and scarcely vegetated catchment inside the active Parinacota setting, Lake Chungará provides a unique record allowing the reconstruction of both natural (volcanic, detrital and natural atmospheric background) and anthropogenic emissions of Hg over the past 2700 years. The contribution of volcanic emissions was estimated as ~30% of the total Hg input to the lake over study period. Due to its western down-wind position, Lake Chungará also recorded regional anthropogenic Hg emissions from both ancient civilizations and more recent Hispanic mining activities. The most recent period strikingly shows that the industrial revolution is of similar magnitude to the largest regional Hg contamination during the colonial mining epoch which commonly overwhelmed local Hg volcanic sources.

Our high-resolution and multiproxy approach validated the value of lake sediment archives to improve the general understanding of Hg deposition and transport pathways, and particularly to quantify local-scale deposition from volcanoes, which is a step further towards better estimation of volcanic Hg emissions. Finally, to refine the quantification of the global volcanic Hg emissions and better constrain proportions of emitted Hg depending on geological context and eruption frequency, similar paleo-limnology approach need to be applied to the main volcanic regions of the globe.

#### Acknowledgements

This work is a contribution to the PALEOBOL project (ISTerre/IRD Program, PI: S. Guédron), which has been supported by a grant from Labex OSUG@2020 (Investissements d'avenir – ANR10 LABX56). We wish to thank A. Castillo and J. Gardon (IRD Bolivia), the Corporación Nacional Forestal (CONAF) of the Arica and Parinacota Region (authorization N°09/2014 - 75059) and the guardaparque personals at Putre CONAF site for their assistance during the field campaigns. We also acknowledge the Umeå Plant Science Centre for making the Py-GC/MS available to us and J. Takahashi Schmidt for the technical support in the Py-GC/MS laboratory. Fieldwork and radiocarbon analyses were supported by NSF EAR-1338694 to S. Fritz and P. Baker. We thank J.-L. Reyss, from the Laboratoire Souterrain de Modane for the gamma spectrometry measurements. We greatly thank the four anonymous reviewers who greatly improved the manuscript with their thoughtful comments.

#### Appendix A. Supplementary data

Supplementary data to this article can be found online at <https://doi.org/10.1016/j.scitotenv.2019.01.294>. The database is also available on Mendeley; <https://data.mendeley.com/datasets/vhvkgz6szf/draft?a=87098869-1e7e-48f6-b0e0-96a60d1f27d7>.

#### References

- Abbott, M.B., Binford, M.W., Brenner, M., Kelts, K.R., 1997. A 3500 14C yr High-Resolution Record of Water-Level Changes in Lake Titicaca, Bolivia/Peru. *Quat. Res.* 47, 169–180.
- Ady, F.D., Patoine, A., 2016. Impacts of land use and climate variability on algal communities since ~1850 CE in an oligotrophic estuary in northeastern New Brunswick, Canada. *J. Paleolimnol.* 55, 151–165.
- Aguilar, P., Dorador, C., Vila, I., Sommaruga, R., 2018. Bacterioplankton composition in tropical high-elevation lakes of the Andean plateau. *FEMS Microbiol. Ecol.* 94, fyy004.
- Amos, H.M., Sonke, J.E., Obrist, D., Robins, N., Hagan, N., Horowitz, H.M., et al., 2015. Observational and modeling constraints on global anthropogenic enrichment of mercury. *Environ. Sci. Technol.* 49, 4036–4047.
- Anselmetti, F.S., Ariztegui, D., De Batist, M., Catalina Gebhardt, A., Haberzettl, T., Niessen, F., et al., 2009. Environmental history of southern Patagonia unravelled by the seismic stratigraphy of Laguna Potrok Aike. *Sedimentology* 56, 873–892.
- Apolinarska, K., Pelechaty, M., Pukacz, A., 2011. Sedimentation by modern charophytes (Characeae): can calcified remains and carbonate  $\delta^{13}\text{C}$  and  $\delta^{18}\text{O}$  record the ecological state of lakes?—a review. *Stud. Limnologica Telmatologica* 5, 55–65.

Bade, D.L., Pace, M.L., Cole, J.J., Carpenter, S.R., 2006. Can algal photosynthetic inorganic carbon isotope fractionation be predicted in lakes using existing models? *Aquat. Sci.* 68, 142–153.

Bagnato, E., Tamburrello, G., Avard, G., Martinez-Cruz, M., Enrico, M., Fu, X., et al., 2014. Mercury fluxes from volcanic and geothermal sources: an update. *Geol. Soc. Lond. Spec. Publ.* 410, 263–285.

Baied, C.A., Wheeler, J.C., 1993. Evolution of high Andean puna ecosystems: environment, climate, and culture change over the last 12,000 years in the Central Andes. *Mt. Res. Dev.* 145–156.

Balslev-Clausen, D., Dahl, T.W., Saad, N., Rosing, M.T., 2013. Precise and accurate  $\delta^{13}\text{C}$  analysis of rock samples using Flash Combustion-Cavity Ring Down Laser Spectroscopy. *J. Anal. At. Spectrom.* 28, 516–523.

Bao, R., Hernandez, A., Saez, A., Giralt, S., Prego, R., Pueyo, J.J., et al., 2015. Climatic and lacustrine morphometric controls of diatom paleoproductivity in a tropical Andean lake. *Quat. Sci. Rev.* 129, 96–110.

Bertrand, Sh., Charlet, Fo., Chapon, E., Fagel, N., De Batist, M., 2008. Reconstruction of the Holocene seismotectonic activity of the Southern Andes from seismites recorded in Lago Icalma, Chile, 39 S. *Palaeogeogr. Palaeoclimatol. Palaeoecol.* 259, 301–322.

Bianchi, T.S., Canuel, E.A., 2011. Chemical Biomarkers in Aquatic Ecosystems. Princeton, Princeton University Press.

Biester, H., Kilian, R., Franzen, C., Woda, C., Mangini, A., Schöler, H.F., 2002. Elevated mercury accumulation in a peat bog of the Magellanic Moorlands, Chile (53°S) – an anthropogenic signal from the Southern Hemisphere. *Earth Planet. Sci. Lett.* 201, 609–620.

Biester, H., Pérez-Rodríguez, M., Gilfedder, B.S., Martínez Cortizas, A., Hermanns, Y.M., 2017. Solar irradiance and primary productivity controlled mercury accumulation in sediments of a remote lake in the Southern Hemisphere during the past 4000 years. *Limnol. Oceanogr.* 63, 540–549.

Blauuw, M., 2010. Methods and code for 'classical' age-modelling of radiocarbon sequences. *Quat. Geochronol.* 5, 512–518.

Brett, C.E., 1990. Obrutton Deposits. Palaeobiology: A Synthesis. Blackwell Scientific, London, pp. 239–243.

Bush, R.T., McInerney, F.A., 2013. Leaf wax n-alkane distributions in and across modern plants: implications for paleoecology and chemotaxonomy. *Geochim. Cosmochim. Acta* 117, 161–179.

Clavero, J., Sparks, R., Huppert, H., Dade, W., 2002. Geological constraints on the emplacement mechanism of the Parinacota debris avalanche, northern Chile. *Bull. Volcanol.* 64, 40–54.

Clavero, R., Jorge, E., Sparks, S.J., Polanco, E., Pringle, M.S., 2004. Evolution of Parinacota volcano, central Andes, northern Chile. *Rev. Geol. Chile* 31, 317–347.

Cole, J.J., Carpenter, S.R., Kitchell, J., Pace, M.L., Solomon, C.T., Weidel, B., 2011. Strong evidence for terrestrial support of zooplankton in small lakes based on stable isotopes of carbon, nitrogen, and hydrogen. *Proc. Natl. Acad. Sci.* 108, 1975–1980.

Cole-Dai, J., Mosley-Thompson, E., Wight, S.P., Thompson, L.G., 2000. A 4100-year record of explosive volcanism from an East Antarctica ice core. *J. Geophys. Res. Atmos.* 105, 24431–24441.

Cooke, C.A., Bindler, R., 2015. Lake sediment records of preindustrial metal pollution. Environmental Contaminants. Springer, pp. 101–119.

Cooke, C.A., Balcom, P.H., Biester, H., Wolfe, A.P., 2009. Over three millennia of mercury pollution in the Peruvian Andes. *Proc. Natl. Acad. Sci.* 106, 8830–8834.

Cooke, C.A., Balcom, P.H., Kerfoot, C., Abbott, M.B., Wolfe, A.P., 2011. Pre-Colombian mercury pollution associated with the smelting of argentiferous ores in the Bolivian Andes. *AMBI* J. Hum. Environ.

Cooke, C.A., Hintemann, H., Ague, J.J., Burger, R., Biester, H., Sachs, J.P., et al., 2013. Use and legacy of mercury in the Andes. *Environ. Sci. Technol.* 47, 4181–4188.

Cruz, P.J., Vacher, J.-J., 2008. Mina y metalurgia en los Andes del Sur: desde la época prehispánica hasta el siglo XVII. Institut de Recherche pour le Développement, La Paz, Bolivia.

Daga, R., Guevara, S.R., Sanchez, M.L., Arribére, M., 2008. Source identification of volcanic ashes by geochemical analysis of well preserved lacustrine tephras in Nahuel Huapi National Park. *Appl. Radiat. Isot.* 66, 1325–1336.

Daga, R., Ribeiro Guevara, S., Pavlin, M., Rizzo, A., Lojen, S., Vreca, P., et al., 2016. Historical records of mercury in southern latitudes over 1600 years: Lake Futalufquen, Northern Patagonia. *Sci. Total Environ.* 553, 541–550.

Damsté, J.S.S., Eglington, T.I., de Leeuw, J.W., 1992. Alkylpyrroles in a kerogen pyrolysis: evidence for abundant tetrapyrrole pigments. *Geochim. Cosmochim. Acta* 56, 1743–1751.

Dorador, C., Vilà, I., Witzel, K.-P., Imhoff, J.F., 2013. Bacterial and archaeal diversity in high altitude wetlands of the Chilean Altiplano. *Fundam. Appl. Limnol.* 182, 135–159.

Engstrom, D.R., Fitzgerald, W.F., Cooke, C.A., Lamborg, C.H., Drevnick, P.E., Swain, E.B., et al., 2014. Atmospheric Hg emissions from preindustrial gold and silver extraction in the Americas: a reevaluation from lake-sediment archives. *Environ. Sci. Technol.* 48, 6533–6543.

Fabbri, D., Adamiano, A., Falini, G., De Marco, R., Mancini, I., 2012. Analytical pyrolysis of dipeptides containing proline and amino acids with polar side chains. Novel 2, 5-diketopiperazine markers in the pyrolysates of proteins. *J. Anal. Appl. Pyrolysis* 95, 145–155.

Ferrara, R., Mazzolai, B., Lanzillotta, E., Nucaro, E., Pirrone, N., 2000. Volcanoes as emission sources of atmospheric mercury in the Mediterranean basin. *Sci. Total Environ.* 259, 115–121.

Fitzgerald, W.F., Gill, G.A., Hewitt, A.D., 1983. Air-sea exchange of mercury. Trace Metals in Sea Water. Springer, pp. 297–315.

France, R.L., 1997. Stable carbon and nitrogen isotopic evidence for ecoregional coupling between boreal forests and fishes. *Ecol. Freshw. Fish* 6, 78–83.

Giralt, S., Moreno, A., Bao, R., Saez, A., Prego, R., Valero-Garcés, B.L., et al., 2008. A statistical approach to disentangle environmental forcings in a lacustrine record: the Lago Chungara case (Chilean Altiplano). *J. Paleolimnol.* 40, 195–215.

Gobeil, C., Cossa, D., 1993. Mercury in sediments and sediment pore water in the Laurentian Trough. *Can. J. Fish. Aquat. Sci.* 50, 1794–1880.

Goldberg, E., 1963. Geochronology with  $^{210}\text{Pb}$ . Radioactive Dating. International Atomic Energy Agency, Vienna, pp. 121–131.

Guédron, S., Grangeon, S., Lanson, B., Grimaldi, M., 2009. Mercury speciation in a tropical soil association; consequence of gold mining on Hg distribution in French Guiana. *Geoderma* 153, 331–346.

Guédron, S., Grimaldi, M., Grimaldi, C., Cossa, D., Tisserand, D., Charlet, L., 2011. Amazonian former gold mined soils as a source of methylmercury: evidence from a small scale watershed in French Guiana. *Water Res.* 45, 2659–2669.

Guédron, S., Amouroux, D., Sabatier, P., Desplanque, C., Develle, A.-L., Barre, J., et al., 2016. A hundred year record of industrial and urban development in French Alps combining Hg accumulation rates and isotope composition in sediment archives from Lake Luitel. *Chem. Geol.* 431, 10–19.

Guédron, S., Point, D., Acha, D., Bouchet, S., Baya, P.A., Molina, C.I., et al., 2017. Mercury contamination level and speciation inventory in the hydrosystem of Lake Titicaca: current status and future trends. *Environ. Pollut.* 231, 262–270.

Guédron, S., Amouroux, D., Tessier, E., Grimaldi, C., Barre, J., Berail, S., et al., 2018a. Mercury isotopic fractionation during pedogenesis in a tropical forest soil catena (French Guiana): deciphering the impact of historical gold mining. *Environ. Sci. Technol.* 52, 11573–11582.

Guédron, S., Ledru, M.P., Escobar-Torrez, K., Develle, A.L., Brisset, E., 2018b. Enhanced mercury deposition by Amazonian orographic precipitation: evidence from high-elevation Holocene records of the Lake Titicaca region (Bolivia). *Palaeogeogr. Palaeoclimatol. Palaeoecol.* 511, 577–587.

Guerrero, S., 2012. Chemistry as a tool for historical research: identifying paths of historical mercury pollution in the Hispanic New World. *Bull. Hist. Chem.* 37, 61–70.

Gustin, M.S., Lindberg, S.E., Weisberg, P.J., 2008. An update on the natural sources and sinks of atmospheric mercury. *Appl. Geochem.* 23, 482–493.

Hellevang, H., Aagaard, P., 2015. Constraints on natural global atmospheric CO<sub>2</sub> fluxes from 1860 to 2010 using a simplified explicit forward model. *Sci. Rep.* 5, 17352.

Hermanns, Y.M., Biester, H., 2013. A 17,300-year record of mercury accumulation in a pristine lake in southern Chile. *J. Paleolimnol.* 49, 547–561.

Hermanns, Y.-M., Cortizas, A.M., Arz, H., Stein, R., Biester, H., 2013. Untangling the influence of in-lake productivity and terrestrial organic matter flux on 4,250 years of mercury accumulation in Lake Hambre, Southern Chile. *J. Paleolimnol.* 49, 563–573.

Hernandez, A., Bao, R., Giralt, S., Leng, M.J., Barker, P.A., Saez, A., et al., 2008. The palaeohydrological evolution of Lago Chungará (Andean Altiplano, northern Chile) during the Lateglacial and early Holocene using oxygen isotopes in diatom silica. *J. Quat. Sci.* 23, 351–363.

Hogg, A.G., Hua, Q., Blackwell, P.G., Niu, M., Buck, C.E., Guilderson, T.P., et al., 2013. SHCal13 Southern Hemisphere calibration, 0–50,000 years cal BP. *Radiocarbon* 55, 1889–1903.

Hora, J.M., Singer, B.S., Wörner, G., 2007. Volcano evolution and eruptive flux on the thick crust of the Andean Central Volcanic zone: 40Ar/39Ar constraints from Volcán Parinacota, Chile. *Geol. Soc. Am. Bull.* 119, 343–362.

Howard, D., Nelson, P.F., Edwards, G.C., Morrison, A.L., Fisher, J.A., Ward, J., et al., 2017. Atmospheric mercury in the Southern Hemisphere tropics: seasonal and diurnal variations and influence of inter-hemispheric transport. *Atmos. Chem. Phys.* 17, 11623–11636.

Hua, Q., Barbetti, M., Rakowski, A.Z., 2013. Atmospheric radiocarbon for the period 1950–2010. *Radiocarbon* 55, 2059–2072.

Ishiwatari, M., Ishiwatari, R., Sakashita, H., Tatsumi, T., Tominaga, H.-O., 1991. Pyrolysis of chlorophyll a after preliminary heating at a moderate temperature: implications for the origin of prist-1-ene on kerogen pyrolysis. *J. Anal. Appl. Pyrolysis* 18, 207–218.

Jokic, A., Schulten, H.R., Cutler, J.N., Schnitzer, M., Huang, P.M., 2004. A significant abiotic pathway for the formation of unknown nitrogen in nature. *Geophys. Res. Lett.* 31.

Kaal, J., Martínez Cortizas, A., Nierop, K.G.J., 2009. Characterisation of aged charcoal using a coil probe pyrolysis-GC/MS method optimised for black carbon. *J. Anal. Appl. Pyrolysis* 85, 408–416.

Kaal, J., Wagner, S., Jaffé, R., 2016. Molecular properties of ultrafiltered dissolved organic matter and dissolved black carbon in headwater streams as determined by pyrolysis-GC-MS. *J. Anal. Appl. Pyrolysis* 118, 181–191.

Körtzinger, A., Quay, P.D., Sonnerup, R.E., 2003. Relationship between anthropogenic CO<sub>2</sub> and the  $^{13}\text{C}$  Suess effect in the North Atlantic Ocean. *Glob. Biogeochem. Cycles* 17.

Kraemer, B.M., Chandra, S., Dell, A.J., Dix, M., Kuusisto, E., Livingstone, D.M., et al., 2017. Global patterns in lake ecosystem responses to warming based on the temperature dependence of metabolism. *Glob. Chang. Biol.* 23, 1881–1890.

Lacerda, L.D., 1997. Global mercury emissions from gold and silver mining. *Water Air Soil Pollut.* 97.

Lacerda, L.D., Ribeiro, M.G., Cordeiro, R.C., Sifeddine, A., Turcq, B., 1999. Atmospheric mercury deposition over Brazil during the past 30,000 years. *Cienc. Cult.* 51, 363–371.

Lacerda, L.D., Turcq, B., Sifeddine, A., Cordeiro, R.C., 2017. Mercury accumulation rates in Caço Lake, NE Brazil during the past 20,000 years. *J. S. Am. Earth Sci.* 77, 42–50.

Lahsen, A., Rojas, J., Morata, D., Aravena, D., 2015. Exploration for high-temperature geothermal resources in the Andean countries of South America. Proceedings of the World Geothermal Congress. Springer International Geothermal Association, Melbourne, Australia, pp. 19–25.

Lamborg, C.H., Fitzgerald, W.F., O'Donnell, J., Torgersen, T., 2002. A non-steady-state compartmental model of global-scale mercury biogeochemistry with interhemispheric atmospheric gradients. *Geochim. Cosmochim. Acta* 66, 1105–1118.

Lechtman, H., 2003. Tiwanaku period (Middle Horizon) bronze metallurgy in the Lake Titicaca Basin: a preliminary assessment. *Tiwanaku and Its Hinterland*. 2, pp. 404–497.

Lechtman, H., 2014. Andean Metallurgy in Prehistory. *Archaeometallurgy in Global Perspective: Methods and Syntheses*. Springer New York, New York, NY, pp. 361–422.

Lechtman, H.N., Macfarlane, A.W., 2005. La metalurgia del bronce en los Andes Sur Centrales: Tiwanaku y San Pedro de Atacama. *Estudios atacameños*. 30 pp. 7–27.

Lindberg, S., Bullock, R., Ebinghaus, R., Engstrom, D., Feng, X., Fitzgerald, W., et al., 2007. A synthesis of progress and uncertainties in attributing the sources of mercury in deposition. *AMBI* J. Hum. Environ.

Lindqvist, O., Rodhe, H., 1985. Atmospheric mercury - a review. *Tellus* B 37, 136–159.

Lohman, K., Seigneur, C., Gustin, M., Lindberg, S., 2008. Sensitivity of the global atmospheric cycle of mercury to emissions. *Appl. Geochem.* 23, 454–466.

Loux, N.T., 1998. An assessment of mercury-species-dependent binding with natural organic carbon. *Chem. Speciat. Bioavailab.* 10, 127–136.

Malm, O., Castro, M.B., Bastos, W.R., Branches, F.J.P., Guimaraes, J.R.D., Zuffo, C.E., et al., 1995. An assessment of Hg pollution in different goldmining areas, Amazon Brazil. *Sci. Total Environ.* 175, 127–140.

Marchant, R., Hooghiemstra, H., 2004. Rapid environmental change in African and South American tropics around 4000 years before present: a review. *Earth Sci. Rev.* 66, 217–260.

Martin, R.S., Witt, M.L.I., Pyle, D.M., Mather, T.A., Watt, S.F.L., Bagnato, E., et al., 2011. Rapid oxidation of mercury (Hg) at volcanic vents: insights from high temperature thermodynamic models of Mt Etna's emissions. *Chem. Geol.* 283, 279–286.

Martin, R.S., Witt, M.L.I., Sawyer, G.M., Thomas, H.E., Watt, S.F.L., Bagnato, E., et al., 2012. Bioindication of volcanic mercury (Hg) deposition around Mt. Etna (Sicily). *Chem. Geol.* 310, 12–22.

Mason, R.P., Choi, A.L., Fitzgerald, W.F., Hammerschmidt, C.R., Lamborg, C.H., Soerensen, A.L., et al., 2012. Mercury biogeochemical cycling in the ocean and policy implications. *Environ. Res.* 119, 101–117.

Meyers, P.A., Ishiwatari, R., 1993. Lacustrine organic geochemistry - an overview of indicators of organic matter sources and diagenesis in lake sediments. *Org. Geochem.* 20, 867–900.

Michelutti, N., Wolfe, A.P., Vinebrooke, R.D., Rivard, B., Briner, J.P., 2005. Recent primary production increases in arctic lakes. *Geophys. Res. Lett.* 32.

Mladinic, P., Hrepic, N., Quintana, E.H., 1987. Caracterización física y química de las aguas de los lagos Chungara y Cotacotani. *Arch. Biol. Med. Exp.* 20, 89–94.

Moreno, A., Giralt, S., Valero-Garcés, B., Sáez, A., Bao, R., Prego, R., et al., 2007. A 14 kyr record of the tropical Andes: the Lago Chungará sequence ( $18^{\circ}$  S, northern Chilean Altiplano). *Quat. Int.* 161, 4–21.

Mucci, A., Bernier, G., Guignard, C., 2015. Mercury remobilization in Saguenay Fjord (Quebec, Canada) sediments: insights following a mass-flow event and its capping efficiency. *Appl. Geochem.* 54, 13–26.

Mühlhauser, H., Hrepic, N., Mladinic, P., Montecino, V., Cabrera, S., 1995. Water quality and limnological features of a high altitude Andean lake, Chungará, in northern Chile. *Rev. Chil. Hist. Nat.* 68, 341–349.

Ninnes, S., Tolu, J., Meyer-Jacob, C., Mighall, T.M., Bindler, R., 2017. Investigating molecular changes in organic matter composition in two Holocene lake-sediment records from central Sweden using pyrolysis-GC/MS. *J. Geophys. Res. Biogeosci.* 122, 1423–1438.

Nriagu, J.O., 1994. Mercury pollution from the past mining of gold and silver in the Americas. *Sci. Total Environ.* 149, 167–181.

Nriagu, J., Becker, C., 2003. Volcanic emissions of mercury to the atmosphere: global and regional inventories. *Sci. Total Environ.* 304, 3–12.

Ohba, T., Hirabayashi, J.-i., Nogami, K., 1994. Water, heat and chloride budgets of the crater lake, Yugama at Kusatsu-Shirane volcano, Japan. *Geochem. J.* 28, 217–231.

Outridge, P.M., Mason, R.P., Wang, F., Guerrero, S., Heimbürger-Boavida, L.E., 2018. Updated global and oceanic mercury budgets for the United Nations Global Mercury Assessment 2018. *Environ. Sci. Technol.* 52, 11466–11477.

Pacyna, E.G., Pacyna, J.M., Steenhuisen, F., Wilson, S., 2006. Global anthropogenic mercury emission inventory for 2000. *Atmos. Environ.* 40, 4048–4063.

Pasternack, G.B., Varekamp, J.C., 1997. Volcanic lake systematics I. Physical constraints. *Bull. Volcanol.* 58, 528–538.

Paul, D., Skrzypek, G., Forizs, I., 2007. Normalization of measured stable isotopic compositions to isotope reference scales-a review. *Rapid Communications in Mass Spectrometry: An International Journal Devoted to the Rapid Dissemination of Up-to-the-Minute Research in Mass Spectrometry*. 21, pp. 3006–3014.

Peulvé, S., Sicre, M., Saliot, A., De Leeuw, J.W., Baas, M., 1996. Molecular characterization of suspended and sedimentary organic matter in an Arctic delta. *Limnol. Oceanogr.* 41, 488–497.

Pirrone, N., Mason, R., 2009. Mercury Fate and Transport in the Global Atmosphere. 10. Springer, Dordrecht, The Netherlands (978-0).

Pirrone, N., Cinnirella, S., Feng, X., Finkelman, R.B., Friedli, H.R., Leaner, J., et al., 2010. Global mercury emissions to the atmosphere from natural and anthropogenic sources. In: Pirrone NaM, R. (Ed.), *Mercury Fate and Transport in the Global Atmosphere*. 1. Springer, pp. 3–50.

Pueyo, J.J., Sáez, A., Giralt, S., Valero-Garcés, B.L., Moreno, A., Bao, R., et al., 2011. Carbonate and organic matter sedimentation and isotopic signatures in Lake Chungará, Chilean Altiplano, during the last 12.3 kyr. *Palaeogeogr. Palaeoclimatol. Palaeoecol.* 307, 339–355.

Pyle, D.M., Mather, T.A., 2003. The importance of volcanic emissions for the global atmospheric mercury cycle. *Atmos. Environ.* 37, 5115–5124.

Rabaté, A., Francou, B., Soruco, A., Gomez, J., Caceres, B., Ceballos, J.L., et al., 2013. Current state of glaciers in the tropical Andes: a multi-century perspective on glacier evolution and climate change. *Cryosphere* 7, 81–102.

Reyss, J.L., Schmid, S., Legeleux, F., Bonte, P., 1995. Large low background well type detectors for measurements of environmental radioactivity. *Nucl. Inst. Methods Phys. Res. B* 391–397.

Ribeiro Guevara, S., Meili, M., Rizzo, A., Daga, R., Arribére, M., 2010. Sediment records of highly variable mercury inputs to mountain lakes in Patagonia during the past millennium. *Atmos. Chem. Phys.* 10, 3443–3453.

Richter, T.O., Van der Gaast, S.J., Koster, B., Vaars, A.J., Gieles, R., De Stigter, H.C., et al., 2006. The Avaatech XRF Core Scanner: technical description and applications to NE Atlantic sediments. In: Rothwell, R.G. (Ed.), *New Techniques in Sediment Core Analysis*. Geological Society, London, pp. 39–50.

Risacher, F., Alonso, H., Salazar, C., 1999. *Geoquímica de aguas en cuencas cerradas: I, II, III Regiones, Chile*. 1. Ministerio de Obras Públicas, Chile, p. 209.

Roos-Barracough, F., Martinez-Cortizas, A., García-Rodeja, E., Shotyk, W., 2002. A 14,500 year record of the accumulation of atmospheric mercury in peat: volcanic signals, anthropogenic influences and a correlation to bromine accumulation. *Earth Planet. Sci. Lett.* 202, 435–451.

Rydberg, J., Gálman, V., Renberg, I., Bindler, R., Lambertsson, L., Martinez-Cortizas, A., 2008. Assessing the stability of mercury and methylmercury in a varved lake sediment deposit. *Environ. Sci. Technol.* 42, 4391–4396.

Sabatier, P., Dezieule, L., Blanchemache, P., Siant, G., Condomines, M., Bentaleb, I., et al., 2010. Holocene variations of radiocarbon reservoir ages in a Mediterranean lagoonal system. *Radiocarbon* 52, 91.

Saez, A., Valero-Garcés, B., Moreno, A., Bao, R., Pueyo, J., Gonzalez-Samperiz, P., et al., 2007. Lacustrine sedimentation in an active volcanic settings: the Late Quaternary depositional evolution of Lake Chungara (northern Chile). *Sedimentology* 1191–1222.

Samaniego, P., Rivera, M., Mariño, J., Guillou, H., Liorzou, C., Zerathé, S., et al., 2016. The eruptive chronology of the Ampato-Sabancaya volcanic complex (Southern Peru). *J. Volcanol. Geotherm. Res.* 323, 110–128.

Sandri, L., Thouret, J.-C., Constantinescu, R., Biass, S., Tonini, R., 2014. Long-term multi-hazard assessment for El Misti volcano (Peru). *Bull. Volcanol.* 76, 771.

Schellekens, J., Buurman, P., Pontevedra-Pombal, X., 2009. Selecting parameters for the environmental interpretation of peat molecular chemistry - a pyrolysis-GC/MS study. *Org. Geochem.* 40, 678–691.

Selin, N.E., 2009. Global biogeochemical cycling of mercury: a review. *Annu. Rev. Environ. Resour.* 34, 43–63.

Shotyk, W., Krachler, M., Martinez-Cortizas, A., Cheburkin, A.K., Emons, H., 2002. A peat bog record of natural, pre-anthropogenic enrichments of trace elements in atmospheric aerosols since 12,370 14C yr BP, and their variation with Holocene climate change. *Earth Planet. Sci. Lett.* 199, 21–37.

Slemr, F., Schuster, G., Seiler, W., 1985. Distribution, speciation, and budget of atmospheric mercury. *J. Atmos. Chem.* 3, 407–434.

Soto Cardenas, C., Gerea, M., Queimalinos, C., Ribeiro Guevara, S., Diéguez, M.C., 2018. Inorganic mercury ( $Hg^{2+}$ ) accumulation in autotrophic and mixotrophic planktonic protists: implications for Hg trophodynamics in ultraoligotrophic Andean Patagonian lakes. *Chemosphere* 199, 223–231.

Stern, C.R., 2008. Holocene tephrochronology record of large explosive eruptions in the southernmost Patagonian Andes. *Bull. Volcanol.* 70, 435–454.

Stewart, C., Johnston, D.M., Leonard, G.S., Horwell, C.J., Thordarson, T., Cronin, S.J., 2006. Contamination of water supplies by volcanic ashfall: a literature review and simple impact modelling. *J. Volcanol. Geotherm. Res.* 158, 296–306.

Stoffers, P., Hannington, M., Wright, I., Herzig, P., De Ronde, C., 1999. Elemental mercury at submarine hydrothermal vents in the Bay of Plenty, Taupo volcanic zone, New Zealand. *Geology* 27, 931–934.

Thevenon, F., Guédron, S., Chiariotti, M., Loizeau, J.-L., Poté, J., 2011. (Pre-)historic changes in natural and anthropogenic heavy metals deposition inferred from two contrasting Swiss Alpine lakes. *Quat. Sci. Rev.* 30, 224–233.

Thompson, L.G., Davis, M.E., Mosley-Thompson, E., Sowers, T.A., Henderson, K.A., Zagorodnov, V.S., et al., 1998. A 25,000-year tropical climate history from Bolivian ice cores. *Science* 282, 1858–1864.

Thouret, J.-C., Davila, J., Eissen, J.-P., 1999. Largest explosive eruption in historical times in the Andes at Huaynaputina volcano, AD 1600, southern Peru. *Geology* 27, 435–438.

Tolu, J., Gerber, L., Boily, J.-F., Bindler, R., 2015. High-throughput characterization of sediment organic matter by pyrolysis gas chromatography/mass spectrometry and multivariate curve resolution: a promising analytical tool in (paleo) limnology. *Anal. Chim. Acta* 880, 93–102.

Tolu, J., Rydberg, J., Meyer-Jacob, C., Gerber, L., Bindler, R., 2017. Spatial variability of organic matter molecular composition and elemental geochemistry in surface sediments of a small boreal Swedish lake. *Biogeosciences* 14, 1773–1792.

Valero-Garcés, B.L., Grosjean, M., Schwab, A., Kelts, K., Schreier, H., Messerli, B., 1996. Limnogeología de laguna Chungara y cambio climático durante el Holoceno superior en el altiplano chileno septentrional. *Cadernos do Laboratorio Xeoloxico de Laxe: Revista de xeoloxoa galega e do hercínico peninsular*, pp. 271–280.

Valero-Garcés, B.L., Grosjean, M., Kelts, K., Schreier, H., Messerli, B., 1999. Holocene lacustrine deposition in the Atacama Altiplano: facies models, climate and tectonic forcing. *Palaeogeogr. Palaeoclimatol. Palaeoecol.* 151, 101–125.

Van Buren, M., Cohen, C.R., 2010. Technological changes in silver production after the Spanish conquest in Porco, Bolivia. *Boletín del Museo Chileno de Arte Precolombino*. 15, pp. 29–46.

Varekamp, J.C., Buseck, P.R., 1986. Global mercury flux from volcanic and geothermal sources. *Appl. Geochem.* 1, 65–73.

Varekamp, J.C., Pasternack, G.B., Rowe Jr., G.L., 2000. Volcanic lake systematics II. Chemical constraints. *J. Volcanol. Geotherm. Res.* 97, 161–179.

Verburg, P., 2007. The need to correct for the Suess effect in the application of  $\delta^{13}\text{C}$  in sediment of autotrophic Lake Tanganyika, as a productivity proxy in the Anthropocene. *J. Paleolimnol.* 37, 591–602.

von Glasow, R., 2010. Atmospheric chemistry in volcanic plumes. *Proc. Natl. Acad. Sci.* 107, 6594.

Vuillemin, A., Ariztegui, D., Nobbe, G., Schubert, C.J., the Pasado Science T, 2017. Influence of methanogenic populations in Holocene lacustrine sediments revealed by clone libraries and fatty acid biogeochemistry. *Geomicrobiol J.* 31, 285–298.

Walker, G.P.L., 1981. Plinian eruptions and their products. *Bull. Volcanol.* 44, 223.

Weide, D.M., Fritz, S.C., Hastorf, C.A., Bruno, M.C., Baker, P.A., Guédrion, S., et al., 2017. A-6000 yr diatom record of mid-to late Holocene fluctuations in the level of Lago Winaymarca, Lake Titicaca (Peru/Bolivia). *Quat. Res.* 88, 179–192.

Wörner, G., Hammerschmidt, K., Henjes-Kunst, F., Lezaun, J., Wilke, H., 2000. Geochronology ( $40\text{Ar}/39\text{Ar}$ , K-Ar and He-exposure ages) of Cenozoic magmatic rocks from northern Chile (18–22 S): implications for magmatism and tectonic evolution of the central Andes. *Rev. Geol. Chile* 27, 205–240.

Zimmer, A., Meneses, R.I., Rabatel, A., Soruco, A., Dangles, O., Anthelme, F., 2017. Time lag between glacial retreat and upward migration alters tropical alpine communities. *Perspect. Plant Ecol. Evol. Syst.* 30, 89–102.